Signal Density of Left Ventricular Myocardial Segments and Impact of Beam Hardening Artifact: Implications for Myocardial Perfusion Assessment by Multidetector CT Coronary Angiography

Gastón A. Rodríguez-Granillo MD, PhD[1,2]; Miguel A. Rosales MD[1]; Elina Degrossi MD[1]; Alfredo E. Rodriguez MD, PhD, FACC[1]

[1] Department of Cardiovascular Imaging, Otamendi Hospital, Buenos Aires, Argentina

[2] Consejo Nacional de Investigaciones Científicas y Tecnológicas (CONICET)

We declare that Dr. G.A. Rodriguez-Granillo has received a research grant from Philips Healthcare

Total Word count: 4250

Running title: Artifacts during myocardial perfusion MDCT

* Correspondence to: Gastón A. Rodríguez-Granillo MD, PhD

Department of Cardiovascular Imaging

Otamendi Hospital

Azcuenaga 870 (C1115AAB)

Buenos Aires, Argentina

Email: grodriguezgranillo@gmail.com

ABSTRACT

Objective: We sought to explore the normal myocardial signal density (SD) levels during multidetector computed tomography coronary angiography (MDCT-CA) acquisitions and evaluated the impact of beam hardening artifacts.

Background: Since myocardial perfusion by MDCT is based on the myocardial signal density (SD), it is pivotal to determine the normal values of myocardial SD and to identify potential mechanisms of misinterpretation of perfusion defects. In routine MDCT acquisitions, we commonly visualize a considerable SD drop at the posterobasal wall resembling perfusion defects, being attributed to beam hardening artifacts.

Methods: Consecutive asymptomatic patients without history of coronary artery disease (CAD) and low probability of CAD who were referred for MDCT evaluation at our institution due to inconclusive or discordant functional tests constituted the study population. Perfusion defects were defined as a myocardial segment having a SD two standard deviations below the average myocardial SD for the 16 left ventricular American Heart Association (AHA) segments.

Results: Thirty six asymptomatic patients constituted the study population. Myocardial SD was evaluated in 576 American Heart Association (AHA) segments and 36 posterobasal segments. The mean myocardial SD at the posterobasal segment was 53.5±35.1 HU, whereas the mean myocardial SD at the basal, mid and apical myocardium was 97.4±17.3, with significant differences ($p<0.001$) between posterobasal and all AHA segments. Posterobasal "perfusion defects" were identified in 26 (72 %) patients. The only variable associated to the presence of posterobasal SD deficit was the heart rate (61.8±6.2 bpm vs. 56.3±8.1 bpm, $p= 0.04$), whereas body mass index, blood SD of the left and right

ventricles, contrast-to-noise ratio, and the extent of atherosclerosis were not related to the presence of “perfusion defects”.

Conclusions: In an asymptomatic population with no history of coronary artery disease, a myocardial signal density deficit mimicking a perfusion defect is a common finding in the posterobasal wall and is not related to body mass index or scan quality.

Key words: perfusion defect, infarct extension, ischemia, spatial distribution, cardiac, computed tomography

Introduction

Multidetector row computed tomography (MDCT) is a rapidly evolving technology that has been positioned as the non-invasive diagnostic approach with the highest predictive accuracy for the detection of coronary stenosis in selected populations [1, 2]. Nevertheless, recent data suggesting that revascularization does not improve the prognosis of patients with intermediate coronary artery stenosis if the stenosis does not impair flow during stress, renders sole anatomical assessment of coronary stenosis without myocardial perfusion information a very useful albeit insufficient approach for clinical decision making [3]. In this regard, myocardial perfusion imaging has shown to be a useful and accurate tool in the diagnosis and prognosis of patients with coronary artery disease (CAD) [4].

Until recently, noninvasive coronary angiography by MDCT was restricted to the evaluation of coronary stenoses from an anatomical standpoint, whereas the assessment of the functional significance of coronary lesions remained outside of its scope [5]. A number of subsequent studies have challenged this limitation by demonstrating that myocardial perfusion during first-pass, contrast-enhanced MDCT during adenosine stress is feasible and related to microsphere-derived myocardial blood flow [6-11].

The advent of prospectively gated acquisition techniques for 64 slice CT coronary angiography has allowed a significant reduction in dose exposure. Consequently, a combined approach of angiography and myocardial perfusion imaging with MDCT might potentially become feasible at a total radiation dose of less than 10 mSv, particularly for the assessment of patients with established coronary artery disease, who are likely to have diffuse calcification [12,13].

Since the asessement of myocardial perfusion by MDCT is based on the myocardial signal density (SD), it is pivotal to determine the normal values of myocardial SD and to identify

potential mechanisms of misinterpretation of perfusion defects. In routine MDCT acquisitions, we commonly visualize a considerable myocardial SD drop at the posterobasal wall resembling perfusion defects (Figure 1), being attributed to beam hardening artifacts. We therefore explored the myocardial SD levels in asymptomatic patients without history of CAD and evaluated the impact of beam hardening artifacts.

Methods

The present was a single-center, investigator-driven, observational study, that involved consecutive asymptomatic patients without history of CAD and low probability of CAD who were referred for MDCT evaluation at our institution due to inconclusive or discordant functional tests. All patients included were > 18 years old, in sinus rhythm, able to maintain a breath-hold for ≥ 15 seconds, without a history of contrast related allergy, renal failure, or haemodynamic instability. Patients with a pre-scan heart rate > 65 bpm received beta-blockers either as a single oral dose or intravenously. In addition, patients with intrascan mild heart rhythm abnormalities leading to motion artifacts such as premature beats and heart rate < 40 bpm were excluded. Scans were performed using a 64-channel MDCT scanner (Brilliance 64, Philips Healthcare, Cleveland, Ohio, USA). A bolus of 80-120 ml of iodinated contrast material (Optiray®, Ioversol 350 mg/ml, Mallinckrodt, St. Louis, U.S.A.) was injected through an arm vein at 5-6 ml/s. A bolus tracking technique was used to synchronize the arrival of contrast at the level of the coronary arteries with the start of acquisition. Scan parameters of the MDCT acquisitions were a collimation of 64 x 0.625 mm, rotation time 0.42 seconds, tube voltage 120 kV, and effective tube current-time product of 600-1000 mAs corresponding to an approximate mean radiation dose of 12 mSv. An ECG-triggered dose modulation protocol (DoseRight Cardiac, Philips Healthcare, Cleveland, Ohio, USA) was applied to reduce radiation dose during systole whenever deemed possible by the operator [14], with approximate dose saving of 42 % at a heart rate of 60 bpm, yielding an approximate mean effective radiation dose of 7 mSv in these patients. An ECG was recorded simultaneous to the CT scan to enable retrospective gating of the image data. A dedicated cardiac gating algorithm was used that identified the same physiological phases of the cardiac cycle while taking into account the non-linear changes

in the individual cardiac states with the heart rate variations during the CT acquisition [15]. A cardiac adaptive multi-cycle (or multi-segment) reconstruction technique was used that combined data from consecutive cardiac cycles, thus significantly improving temporal resolution between 53 and 210 ms [16].

MDCT analysis

All analyses were performed by consensus of 2 experienced (> 1500 MDCT performed) observers using dedicated software (Comprehensive Cardiac Analysis, version 3.5), on a CT workstation (Brilliance Workspace, Philips Healthcare, Cleveland, Ohio, USA).

MDCT images were reconstructed at 75 % of the cardiac phase using axial planes, multiplanar reconstructions, and maximum intensity projections at 1 mm slice thickness. Short axis views were obtained initially using 5-mm slice reformatted images at the basal, mid ventricle and apical levels. The posterobasal wall (Figure 1), a basal segment not included in the American Heart Association (AHA) 17-segment model [17] , was also evaluated at the short axis plane including the mitral valve and the left ventricular outflow tract (Figure 1). Using standarized regions of interest of 20 mm2, myocardial signal density (SD) was determined for every segment according to the AHA 17-segment model [17] (Figure 2). AHA segment 17 corresponding to the apical wall evaluated from the long axis was excluded from the analysis since it encompasses a thin myocardial wall and is therefore prone to measurement error. Left ventricular and right ventricular chamber mean SD were evaluated at basal, mid and apical short axis.

Definitions

“Perfusion defects” were defined as myocardium having a SD two standard deviations below the mean myocardial SD of the 16 AHA segments. Myocardial SD was evaluated at the posterobasal wall using the same approach. SD ratio, which is highly related to

myocardial blood flow measured by microspheres[6], was determined as previously described: myocardial SD/left ventricular blood pool SD [6].

Myocardial SD and myocardial SD ratios were evaluated for the posterobasal segment and for AHA segments. In addition, myocardial SD and SD ratios were compared between patients with and without "perfusion defects" at the posterobasal wall.

In order to assess image quality and relate it to the presence of beam-hardening artifacts, we determined image noise and contrast-to-noise ratios and evaluated posible associations with posterobasal wall perfusion defects. Image noise was derived from the standard deviation of the SD values (in Hounsfield units) within a large region of interest in the left ventricle. The contrast-to-noise ratio was defined as the difference between the mean density of the contrast-filled left ventricular chamber and the mean density of the left ventricular wall, which was divided by image noise.

The study was approved by our Institution´s Ethics Committee, and all the patients enrolled gave their written informed consent.

Statistical analysis

Discrete variables are presented as counts and percentages. Continuous variables are presented as mean ± SD or median (25th, 75th percentile) as indicated. Comparisons among groups were performed using paired samples t-test, independent samples t-test, analysis of variance (ANOVA), chi square tests, Fisher´s exact test, or Mann-Whitney U tests as indicated. We explored correlations between the posterobasal wall SD and variables thought to be related to the presence beam hardening artifacts using Spearman correlation coefficients. A two-sided p value of less than 0.05 indicated statistical significance. Statistical analyses were performed with use of SPSS software, version 13.0 (Chicago, Illinois, USA).

Results

Thirty six asymptomatic patients constituted the study population. The mean age was 55.9±10.6 years, 29 (81 %) were male and 1 (3 %) was diabetic.

Myocardial SD was evaluated in 576 AHA segments and 36 posterobasal segments. The mean myocardial SD at the posterobasal segment was 53.5±35.1 HU, whereas the mean myocardial SD at the basal, mid and apical myocardium was 97.4±17.3, with significant differences ($p<0.001$) between posterobasal and all AHA segments (Table 1). Similarly, myocardial SD ratio at the posterobasal segment was 0.14±0.09, whereas the SD ratio at the basal, mid and apical myocardium was 0.25±0.06, with significant differences ($p<0.001$) between posterobasal and all AHA segments (Table 2). With regard to the spatial distribution of SD, the septal segments (AHA 2, 3, 8, 9 and 14) had significantly higher myocardial SD than the other segments (Table 3).

Posterobasal "perfusion defects"

Posterobasal "perfusion defects" at at the short axis plane including the mitral valve and the left ventricular outflow tract, were identified in 26 (72 %) patients (Figure 1, Table 1). In addition, though infrequently, perfusion defects were identified at several AHA segments, particularly at segments 4, 5 and 13, corresponding to the inferobasal (segments 4 and 5) and anteroapical walls, with a prevalence of 11 %, 17 % and 17 %, respectively (Table 1). The only demographical variable associated to the presence of posterobasal "perfusion defects" was heart rate (61.8±6.2 bpm vs. 56.3±8.1 bpm, p= 0.04), whereas body mass index (BMI) was not related to the presence of perfusion defects (28.0±3.7 kg/m^2 vs. 27.1±4.6 kg/m^2, p= 0.55). Blood densities of the left and right ventricular chambers were not associated to the presence of posterobasal "perfusion defects" (Table 4). In addition, contrast-to-noise ratio and signal noise were not related to the presence of "perfusion

defects" (Table 4). Regarding the presence and extent of coronary atherosclerosis, patients with posterobasal "perfusion defects" had similar Agatston calcium scores (0.0 (0.0-29.5) vs. 0.0 (0.0-259.0), p= 0.81), number of lesions (1.5±2.6 vs. 1.7±2.5, p= 0.81) and number of significant lesions (0.2±0.6 vs. 0.4±1.3, p= 0.63) than patients without posterobasal "perfusion defects".

Finally, we did not find a significant relationship between posterobasal wall SD and heart rate (r= -0.16, p= 0.37), BMI (r= -0.12, p= 0.49), basal left ventricular chamber SD (r= 0.16, p= 0.35), basal right ventricular chamber SD (r= 0.16, p= 0.36), basal signal noise (r= -0.05, p= 0.79), basal contrast-to-noise ratio (r= 0.14, p= 0.42), and calcium score (r= 0.10, p= 0.55). In turn, a weak positive correlation was identified between posterobasal wall SD and descending aorta SD (r= 0.35, p= 0.04).

Discussion

For decades, myocardial perfusion imaging has been undoubtedly established as the gold-standard for prognosis and clinical decision making of patients with CAD, and has predominantly been assessed by single-positron emission tomography (SPECT) and, more recently, by positron emission tomography and magnetic resonance imaging (MRI).

After standing as an accurate tool to evaluate coronary stenosis in a non-invasive fashion, several non-coronary applications of MDCT have emerged and were tested with success, including myocardial function, viability and perfusion [8-11, 17-20]. Among them, myocardial perfusion imaging by MDCT has been explored by a number of preclinical and clinical studies showing that hypoenhanced regions on contrast-enhanced MDCT correlate well to hypoperfused myocardial regions, becoming an accurate tool to evaluate myocardial infarction, with a good agreement with gated SPECT and MRI [6-11, 21,22]. The pathophysiological basis of this concept is based on the kinetics of the iodinated contrast agent used for MDCT that, parallel to gadolinium-DTPA in contrast enhanced magnetic resonance, has a decreased inflow to the myocardium in the setting of a coronary stenosis, resulting in early hypoenhancement during contrast inflow [6,23].

The present study is the first to establish the normal values of myocardial SD of left ventricular segments in an asymptomatic population, as well as SD values normalized according to the left ventricular chamber SD (SD ratio). Acquaintance of these normal values and identification of artifacts mimicking perfusion defects is essential to avoid misinterpretation of myocardial perfusion by MDCT. Our main findings can be summarized as follows:

- Beam hardening artifacts are a common finding in MDCT-CA of asymptomatic patients, and affect predominantly the posterobasal wall appearing as myocardial perfusion defects.
- "Perfusion defects" at the short axis plane including the mitral valve and the left ventricular outflow tract were not related to technical issues such as BMI, contrast in the aorta, right ventricle, contrast-to noise ratio or signal noise, whereas heart rate was associated with this finding.
- Although very rarely, myocardial "perfusion defects" can be identified at the inferior and anteroapical segments of the left ventricular wall.

We identified a high prevalence of SD deficit at the posterobasal wall resembling perfusion defects. It should be stressed however, that SD deficit was commonly identified opposite to the left ventricular outflow tract, a segment not included in the AHA classification.

In addition, we found a trend towards lower myocardial SD, and even a few perfusion defects at the anteroapical and inferior (mid and basal) segments of the left ventricular wall. We ascribe this finding to beam-hardening artifact most probably from the spine for posterobasal segments and from the sternum for anteroapical segments that have an appearance similar to a myocardial perfusion deficit in contrast-enhanced coronary CTA images. The selective filtration of low-energy photons by highly attenuating cardiac structures, such as the contrast-enhanced left ventricle, the descending aorta, and occasionally the right ventricle, as well as bony structures such as the spine, sternum, and ribs, may create focal areas of nonphysiologic hypoenhancement in the myocardium. Since all these highly attenuating structures are aligned along the same x-ray path as these myocardial segments, we typically see worse beam hardening selectively in posterobasal segments. That being said, contrary to what it was expected, technical issues such as

contrast in the right and left ventricular chambers, contrast-to-noise ratio, signal noise and BMI, as well as the presence and extent of coronary atherosclerosis, were not related to the presence of perfusion defects in our study. Nevertheless, patients with lower heart rate were more likely to have normal SD, although we did not find a significant relationship between posterobasal wall SD and heart rate.

Occurrence of attenuation artifacts during SPECT imaging has been considered an important limitation of the technique [24]. Our results indicate that attenuation artifacts also occur in MDCT perfusion imaging and should be accounted for in order to avoid being misinterpreted as perfusion defects.

Limitations

Although we included asymptomatic patients with no history of CAD and small, if any, atherosclerotic burden, confirmation of the absence of ischemia with SPECT or MRI was not performed. In addition we did not use 2-phase or 3-phase contrast injection protocols with saline to minimize right-heart contrast. Nevertheless, we did not find an association between the presence of contrast in the right ventricular chamber and perfusion defects.

Finally, image acquisition requires a number of heart beats leading to potential non-uniform distribution of contrast in myocardial segments. Nevertheless, blood signal density at both left and right ventricles (at basal, mid and apical levels), as well as at the ascending and descending aorta, did not differ between patients with and without SD deficit. In addition, acquisition time were similar in patients with and without “perfusion defects” therefore the number of cardiac cycles probably were not associated to the presence of defects.

Conclusions

In an asymptomatic population with no history of coronary artey disease, myocardial signal density deficit mimicking perfusion defects is a common finding at the posterobasal wall and is not related to body mass index or scan quality.

Acknowledgements

We would like to thank Dr. Eduardo Diez, Jonathan Lessick, Thomas Ivanc and Mani Vembar for their generous contribution to the study.

References

1. Budoff MJ, Dowe D, Jollis JG, Gitter M, Sutherland J, Halamert E, Scherer M, Bellinger R, Martin A, Benton R, Delago A, Min JK. Diagnostic Performance of 64-Multidetector Row Coronary Computed Tomographic Angiography for Evaluation of Coronary Artery Stenosis in Individuals Without Known Coronary Artery Disease Results From the Prospective Multicenter ACCURACY (Assessment by Coronary Computed Tomographic Angiography of Individuals Undergoing Invasive Coronary Angiography) Trial. J Am Coll Cardiol 2008;52:1724–32.
2. Miller JM, Rochitte CE, Dewey M, Arbab-Zadeh A, Niinuma H, Gottlieb I, Paul N, Clouse ME, Shapiro EP, Hoe J, Lardo AC, Bush DE, Roos A, Cox C, Brinker J, Lima JAC. Diagnostic Performance of Coronary Angiography by 64-Row CT. N Engl J Med 2008;359:2324-36.
3. Pijls NH, van Schaardenburgh P, Manoharan G, et al. Percutaneous coronary intervention of functionally nonsignificant stenosis: 5-year follow-up of the DEFER study. J Am Coll Cardiol 2007;49:2105–11.
4. Klocke FJ, Baird MG, Lorell BH, et al. ACC/AHA/ASNC guidelines for the clinical use of cardiac radionuclide imaging—executive summary: a report of the American College of Cardiology/American Heart Association Task Force on Practice Guidelines (ACC/AHA/ASNC Committee to Revise the 1995 Guidelines for the Clinical Use of Cardiac Radionuclide Imaging). J Am Coll Cardiol 2003;42:1318 –33.
5. Meijboom WB, Van Mieghem CA, van Pelt N, Weustink A, Pugliese F, Mollet NR, Boersma E, Regar E, van Geuns RJ, de Jaegere PJ, Serruys PW, Krestin

GP, de Feyter PJ. Comprehensive assessment of coronary artery stenoses: computed tomography coronary angiography versus conventional coronary angiography and correlation with fractional flow reserve in patients with stable angina. J Am Coll Cardiol. 2008 Aug 19;52(8):636-43.

6. George RT, Silva C, Cordeiro MAS, Di Paula A, Thompson DR, McCarthy WF, Ichihara T, Lima JAC, Lardo AC. Multidetector computed tomography myocardial perfusion imaging during adenosine stress. J Am Coll Cardiol 2006;48:153– 60.

7. George RT, Jerosch-Herold M, Silva C, et al. Quantification of myocardial perfusion using dynamic 64-detector computed tomography. Invest Radiol 2007;42:815–22.

8. Gerber BL, Belge B, Legros GJ, Lim P, Poncelet A, Pasquet A, Gisellu G, Coche E, Vanoverschelde JL. Characterization of acute and chronic myocardial infarcts by multidetector computed tomography: comparison with contrast-enhanced magnetic resonance. Circulation. 2006;113(6):823-833.

9. Lardo AC, Cordeiro MA, Silva C, Amado LC, George RT, Saliaris AP, Schuleri KH, Fernandes VR, Zviman M, Nazarian S, Halperin HR, Wu KC, Hare JM, Lima JA. Contrast-enhanced multidetector computed tomography viability imaging after myocardial infarction: characterization of myocyte death, microvascular obstruction, and chronic scar. Circulation. 2006;113(3):394-404.

10. Blankstein R, Shturman LD, Rogers IS, Rocha-Filho JA, Okada DR, Sarwar A, Soni AV, Bezerra H, Ghoshhajra BB, Petranovic M, Loureiro R, Feuchtner G, Gewirtz H, Hoffmann U, Mamuya WS, Brady TJ, Cury RC. Adenosine-induced

stress myocardial perfusion imaging using dual-source cardiac computed tomography. J Am Coll Cardiol. 2009; 54(12):1072-84.

11. Mahnken AH, Koos R, Katoh M, Wildberger JE, Spuentrup E, Buecker A, Gunther RW, Kuhl HP. Assessment of myocardial viability in reperfused acute myocardial infarction using 16-slice computed tomography in comparison to magnetic resonance imaging. J Am Coll Cardiol. 2005;45(12):2042-2047.
12. Herzog BA, Husmann L, Burkhard N, Gaemperli O, Valenta I, Tatsugami F, Wyss CA, Landmesser U, Kaufmann PA. Accuracy of low-dose computed tomography coronary angiography using prospective electrocardiogram-triggering: first clinical experience. Eur Heart J. 2008 Dec;29(24):3037-42.
13. Nagel E, Lima JAC, George RT. Newer Methods for Noninvasive Assessment of Myocardial Perfusion Cardiac Magnetic Resonance or Cardiac Computed Tomography? J. Am. Coll. Cardiol. Img. 2009;2;656-660.
14. Hausleiter J, Meyer T, Hadamitzky M, Huber E, Zankl M, Martinoff S, Kastrati A, Schomig A. Radiation dose estimates from cardiac multislice computed tomography in daily practice: impact of different scanning protocols on effective dose estimates. Circulation. 2006;113(10):1305-1310.
15. Vembar M, Garcia MJ, Heuscher DJ, Haberl R, Matthews D, Bohme GE, et al. A dynamic approach to identifying desired physiological phases for cardiac imaging using multislice spiral CT. Med Phys 2003;30(7):1683-93.
16. Manzke R, Grass M, Nielsen T, Shechter G, Hawkes D. Adaptive temporal resolution optimization in helical cardiac cone beam CT reconstruction. Med Phys. 2003; 30:3072-3080.

17. Cerqueira MD, Weissman NJ, Dilsizian V, Jacobs AK, Kaul S, Laskey WK, Pennell DJ, Rumberger JA, Ryan T, Verani MS. Standardized myocardial segmentation and nomenclature for tomographic imaging of the heart: a statement for healthcare professionals from the Cardiac Imaging Committee of the Council on Clinical Cardiology of the American Heart Association. Circulation. 2002;105(4):539-542.

18. Henneman MM, Schuijf JD, Jukema JW, et al. Assessment of global and regional left ventricular function and volumes with 64-slice MSCT: a comparison with 2D echocardiography. J Nucl Cardiol 2006;13:480 –7.

19. Yamamuro M, Tadamura E, Kubo S, et al. Cardiac functional analysis with Multidetector row CT and segmental reconstruction algorithm: comparison with echocardiography, SPECT, and MR imaging. Radiology 2005;234:381–90.

20. Rodriguez-Granillo GA, Rosales MA, Baum S, Rennes P, Rodriguez-Pagani C, Curotto V, Fernandez-Pereira C, Llaurado C, Risau G, Degrossi E, Doval HC, Rodriguez AE. Early Assessment of Myocardial Viability by the Use of Delayed Enhancement Computed Tomography After Primary Percutaneous Coronary Intervention. J. Am. Coll. Cardiol. Img. 2009;2;1072-1081.

21. Hoffmann U, Millea R, Enzweiler C, et al. Acute myocardial infarction: contrast-enhanced multidetector row CT in a porcine model. Radiology 2004;231:697–701.

22. Mahnken AH, Bruners P, Katoh M, Wildberger JE, Gunther RW, Buecker A. Dynamic multi-section CT imaging in acute myocardial infarction: preliminary animal experience. Eur Radiol 2006;16:746–52.

23. Uren NG, Melin JA, De Bruyne B, Wijns W, Baudhuin T, Camici PG. Relation between myocardial blood flow and the severity of coronary-artery stenosis. N Engl J Med 1994;330:1782– 8.

24. Schwitter J, Wacker CM, van Rossum AC, et al. MR-IMPACT: comparison of perfusion-cardiac magnetic resonance with single-photon emission computed tomography for the detection of coronary artery disease in a multicentre, multivendor, randomized trial. Eur Heart J 2008;29:480 –9.

Table 1. Myocardial signal density (Hounsfield units, HU) of left ventricular segments and posterobasal wall, and frequency of perfusion defects defined as myocardium having a signal density two standard deviations below the mean signal density of all left ventricular segments.

		HU (mean ± SD)	p value vs. posterobasal	Perfusion defects
	Posterobasal	53.5±35.1		26 (72 %)
B	**AHA-1**	93.4±16.1	<0.001	0 (0 %)
A	**AHA-2**	101.7±22.8	<0.001	1 (3 %)
S	**AHA-3**	103.5±19.5	<0.001	0 (0 %)
A	**AHA-4**	85.2±19.3	<0.001	4 (11 %)
L	**AHA-5**	87.0±30.6	<0.001	6 (17 %)
	AHA-6	101.1±19.6	<0.001	0 (0 %)
	AHA-7	86.3±18.5	<0.001	3 (8 %)
M	**AHA-8**	112.7±24.0	<0.001	0 (0 %)
I	**AHA-9**	101.6±22.8	<0.001	0 (0 %)
D	**AHA-10**	100.3±20.7	<0.001	1 (3 %)
	AHA-11	103.7±21.1	<0.001	3 (8 %)
	AHA-12	97.5±20.8	<0.001	1 (3 %)
A				
P	**AHA-13**	81.3±21.5	<0.001	6 (17 %)
I	**AHA-14**	109.0±26.9	<0.001	2 (6 %)
C	**AHA-15**	97.7±22.1	<0.001	2 (6 %)
A	**AHA-16**	98.7±22.0	<0.001	1 (3 %)
L				

Table 2. Myocardial signal density ratio of left ventricular segments and posterobasal wall, defined as myocardial signal density/left ventricular chamber signal density.

		Signal density ratio	p value vs. posterobasal
	Posterobasal	0.14±0.09	
B	**AHA-1**	0.24±0.05	<0.001
A	**AHA-2**	0.26±0.05	<0.001
S	**AHA-3**	0.27±0.05	<0.001
A	**AHA-4**	0.22±0.05	<0.001
L	**AHA-5**	0.22±0.08	<0.001
	AHA-6	0.26±0.05	<0.001
	AHA-7	0.22±0.06	<0.001
M	**AHA-8**	0.29±0.06	<0.001
I	**AHA-9**	0.26±0.06	<0.001
D	**AHA-10**	0.26±0.05	<0.001
	AHA-11	0.27±0.06	<0.001
	AHA-12	0.25±0.06	<0.001
A			
P	**AHA-13**	0.21±0.07	<0.001
I	**AHA-14**	0.28±0.06	<0.001
C	**AHA-15**	0.25±0.06	<0.001
A	**AHA-16**	0.26±0.06	<0.001
L			

Table 3. Spatial distribution of myocardial signal density. Septal segments (American Heart Association (AHA) segments# 2, 3, 8, 9 and 14) had significantly higher myocardial signal density than the other segments.

Spatial distribution	**Signal density (HU)**	
Anterior (AHA 1,7,13)	87.0±16.1	
Septal (AHA 2,3,8,9,14)	105.7±19.5	
Inferior (AHA 4,10,15)	94.4±17.6	
Lateral (AHA 5,6,11,12,16)	97.6±18.2	
ANOVA across group	<0.001	
Comparisons between groups (Bonferroni)	Anterior vs. septal	<0.001
	Anterior vs. inferior	0.49
	Anterior vs. lateral	0.08
	Septal vs inferior	0.05
	Septal vs. lateral	0.35
	Inferior vs. lateral	0.99

Table 4. Relationship between patient´s demographics, acquisition parameters, image quality, atherosclerosis and the presence of myocardial signal density deficit mimicking perfusion defects at the posterobasal wall.

	Posterobasal perfusion defect (n=26)	**Normal signal intensity (n= 10)**	**p value**
Demographics			
Heart rate (bpm)	61.8±6.2	56.3±8.1	0.04
Age (years)	55.1±10.9	56.2±10.2	0.78
Male	23 (79 %)	6 (21 %)	0.08
Hypertension	9 (60 %)	6 (40 %)	0.26
Dislipemia	15 (75 %)	5 (25 %)	0.72
Diabetes	0 (0 %)	1 (100 %)	0.28
Previous smoking	6 (86 %)	1 (14 %)	0.42
Current smoking	8 (80 %)	2 (20 %)	
Body mass index (kg/m^2)	28.0±3.7	27.2±4.6	0.55
Acquisition time (sec)	9.6±0.8	9.8±0.7	0.61
Blood signal density in the aorta (Hounsfeld units)			
Aortic root	405.9±66.2	444.8±65.9	0.12
Descending aorta*	391.8±61.8	434.4±59.9	0.08
Blood signal density of the left ventricle (Hounsfield units)			
Basal	378.9±65.2	396.2±50.1	0.45
Mid	381.9±67.5	405.8±57.4	0.33
Apical	402.3±68.1	422.6±64.7	0.42
Blood signal density of the right ventricle (Hounsfield units)			
Basal	175.2±48.6	182.4±38.4	0.68
Mid	186.4±65.4	185.4±42.0	0.97
Apical	227.9±70.4	223.1±61.4	0.85
Myocardial signal density (HU) in LV segments (AHA classification)			
Basal (AHA 1-6)	92.3±15.1	103.2±20.2	0.14
Mid (AHA 7-12)	98.0±16.5	106.3±16.3	0.18
Apical (AHA 13-16)	93.9±17.0	104.0±20.5	0.14
Posterobasal wall myocardial signal density (SD) ratio			
SD ratio	0.10±0.05	0.24±0.08	<0.001
Difference in myocardial signal density between the posterobasal (PB) wall and LV AHA segments (Hounsfield units)			
Δ PB vs. AHA 1-6	55.6±17.8	5.7±27.2	<0.001
Δ PB vs. AHA 7-12	61.4±22.5	8.8±24.6	<0.001
Δ PB vs. AHA 13-16	57.2±21.7	6.5±26.0	<0.001

Contrast-to-noise ratio			
Basal	12.7±5.2	12.6±2.3	0.93
Mid	13.7±3.9	14.7±3.0	0.50
Apical	16.8±6.5	18.4±7.7	0.53
Signal noise			
Aorta	23.5±5.6	22.1±5.0	0.48
Basal LV	24.3±6.1	23.7±4.3	0.78
Mid LV	21.4±4.6	20.8±4.2	0.73
Apical LV	20.1±5.8	19.5±8.2	0.81
Coronary atherosclerosis			
Agatston score	0.0 (0.0-29.5)	0.0 (0.0-259.0)	0.81**
N lesions	1.5±2.6	1.7±2.5	0.81
N significant lesions	0.2±0.6	0.4±1.3	0.63

LV refers to left ventricle. * Adjacent to posterobasal wall. **Mann-Whitney U tests

Figure legends.

Figure 1.

Basal short axis at the left ventricular outflow tract (panel a), conventional basal short axis (panel b), and axial view (panel c) showing decreased myocardial density at the posterobasal wall (arrows) and normal attenuation at the remaining segments.

Figure 2.

Myocardial signal density (above) and signal density ratio (below) levels of left ventricular myocardium segments showing decresed signal density of posterobasal (PB) segments.

Figure 1.

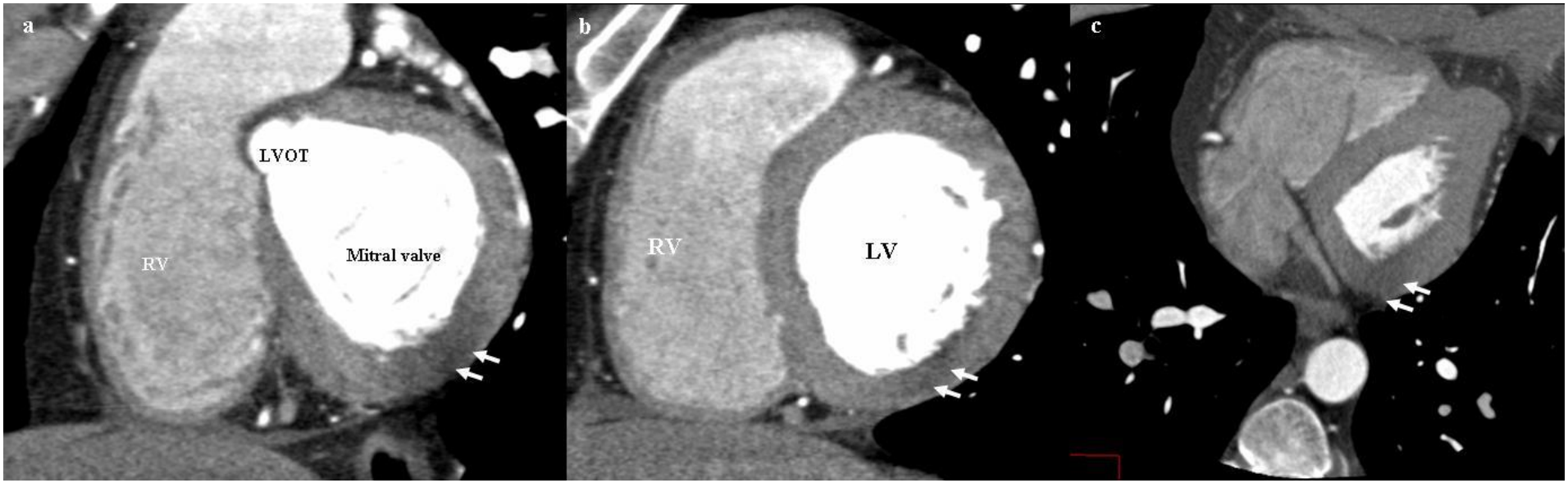

Figure 2.

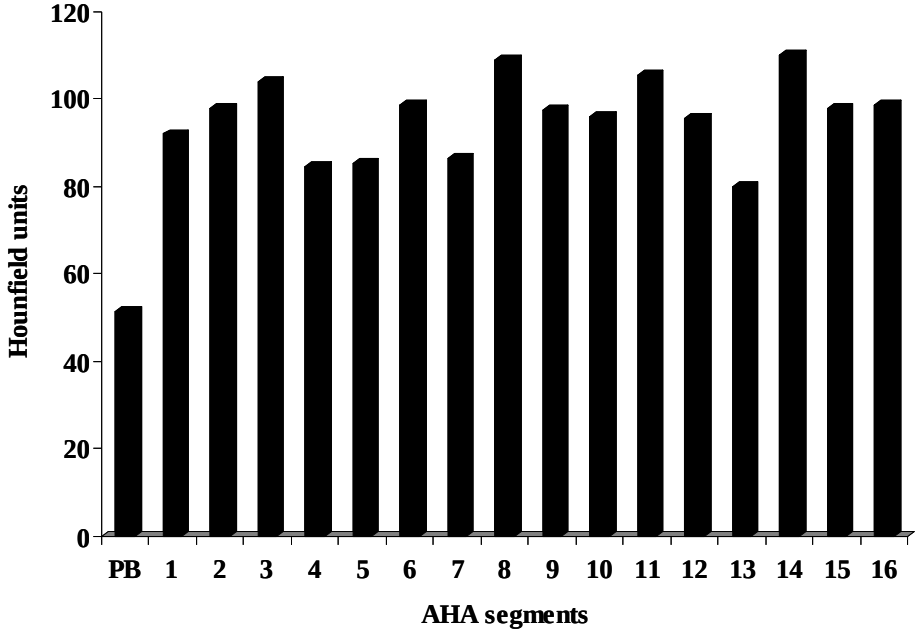

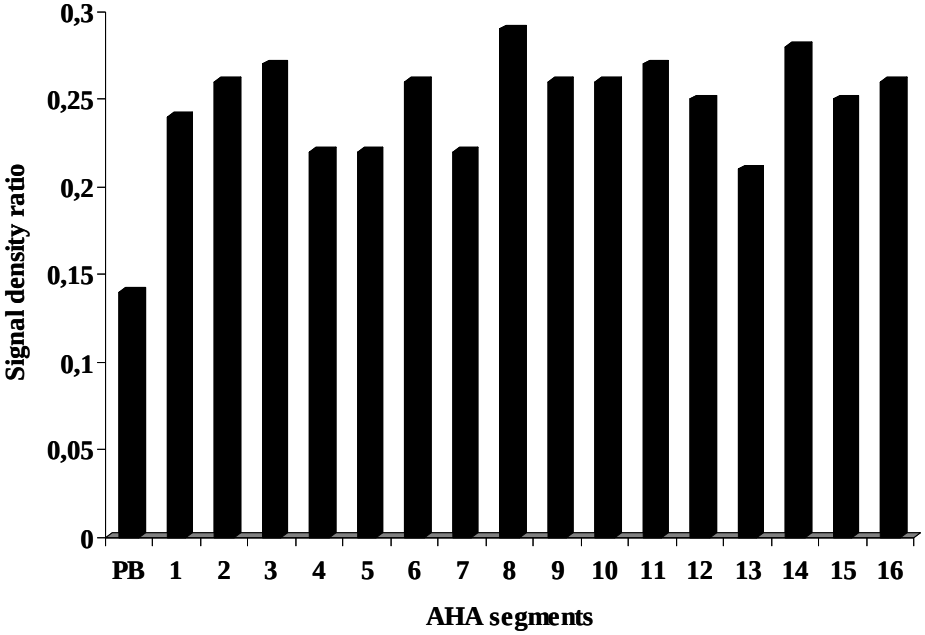

Left ventricular segmentation

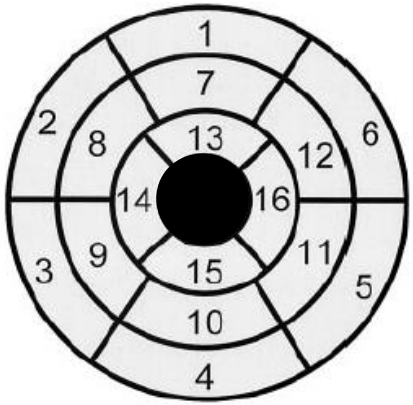

1. Basal anterior
2. Basal anteroseptal
3. Basal inferoseptal
4. Basal inferior
5. Basal inferolateral
6. Basal anterolateral
7. Mid anterior
8. Mid anteroseptal
9. Mid inferoseptal
10. Mid inferior
11. Mid inferolateral
12. Mid anterolateral
13. Apical anterior
14. Apical septal
15. Apical inferior
16. Apical lateral